Journal of Materials Science: Materials in Electronics
https://doi.org/10.1007/s10854-020-03481-w

Improved energy harvesting using well-aligned ZnS nanoparticles in bulk-heterojunction organic solar cell

Mpilo W. Dlamini[1] · Mohammed S. G. Hamed[1] · Xolani G. Mbuyise[1] · Genene T. Mola[1]

Received: 17 February 2020 / Accepted: 25 April 2020

Abstract
Zinc sulphide (ZnS) nanoparticles (NPs) were synthesized by low temperature colloidal chemistry to produce stable zinc blend structure. The metallic ZnS NPs were incorporated into poly(3-hexylthiophene) (P3HT) and (6,6)-phenyl C_{61}-butyric acid methyl ester (PCBM) blend photoactive layer to improve the overall performance of organic solar cells (OSC). The newly fabricated devices have exhibited enhanced photocurrent which is likely to come from utilizing the near-field and light scattering effects due to the NPs. The short-circuit current density of the best solar cell was enhanced to as high as 15.65 mA cm^{-2} followed by 51% and 4.0% maximum fill-factor (FF) and power conversion efficiency (PCE), respectively. This enhancement is very comparable to those obtained from the use of expensive plasmonic gold and silver nanoparticles. The current results are encouraging to improve the performance of OSC through a facile yet cost-effective and environmentally friendly approach of metal nanoparticles synthesis.

1 Introduction

One of the most popular organic molecules blend, that served as a solar absorber medium in OSC, is the mixture of poly(3-hexylthiophene) (P3HT) and (6,6)-phenyl C_{61}-butyric acid methyl ester (PCBM). The power conversion efficiency of this polymer-fullerene combination has grown to as high as 5% [1–5] through utilization of several optimization techniques such as solvent additive, thermal and solvent annealing, and the utilization of localized surface plasmon resonance (LSPR). However, limitations such as low charge carrier mobility, weak photon absorption in the visible spectrum, and low open-circuit voltage (V_{oc}) (~ 0.6 V [6]) still exist in P3HT:PCBM blend-based OSC due to the deep lying lowest unoccupied molecular orbital (LUMO) levels of PCBM [4, 7]. Different approaches have been taken to enhance performance of OPVs while keeping active layer thickness unchanged to avoid increasing charge recombination. Recently, metallic nanoparticles (NPs) are increasingly being introduced into OSC devices for highly improved light harvesting by employing the LSPR effect of metallic nanoparticles [8–10].

The strong electromagnetic fields produced near metallic NPs can inprinciple be expected to enhance the optical absorption in OSCs [11]. We report here a power conversion efficiency increment of more than 50% by the incorporation of plasmonic zinc sulphide (ZnS) NPs in the P3HT:PCBM blend photoactive layer. Zinc sulphide is an environmentally friendly and stable transition metal sulphide which can be synthesized easily and inexpensively [7] using low temperature colloidal chemistry. ZnS nanoparticles show special photoelectric properties, such as photoluminescence and electroluminescence [12]. It is a wide bandgap semiconductor with high electron mobility (600 cm^2 V^{-1} s^{-1}) and has an electron affinity of about 3.9 eV making it an attractive material to use as an electron acceptor in hybrid photovoltaic devices [7]. Bredol et al. used ZnS NPs as electron acceptors and obtained a maximum V_{oc} of 1.2 V when hexagonal ZnS NPs were used in contact with P3HT at a ZnS NPs concentration of 50 wt% [13]. However, the PCE was rather low (0.2%) compared to the conventional BHJ P3HT:PCBM blend devices [7, 13]. The optical properties of ZnS NPs dramatically change due to their quantum confinement effect and improve as compared to their bulk counterparts [14]. Zinc sulphide exhibits polymorphism since it forms two main types of crystal phases, namely the most stable zincblende cubic structure (< 1290 K) and hexagonal phase

✉ Genene T. Mola
mola@ukzn.ac.za

[1] School of Chemistry & Physics, University of KwaZulu-Natal, Pietermaritzburg Campus, Private Bag X01, Scottsville 3209, South Africa

Published online: 11 May 2020

with wurtzite symmetry at high temperature above 1290 K [12, 14–16].

2 Materials and methods

2.1 Materials

Chemical materials used for the fabrication of OPVs were purchased and used as received without further processing except the synthesis of ZnS. Poly(3-hexylthiophene) (P3HT), phenyl-C_{71}-butyric acid methyl ester (PCBM) and PEDOT:PSS were purchased from Ossila Co. Ltd. Zinc acetate and sodium sulphide nanohydrate were purchased from Merck, Germany. Polyvinylpyrrolidone (PVP, $(C_6H_9NO)_n$, MW of 25,000–30,000) LAB.

2.2 Synthesis and characterization of ZnS nanoparticles

The ZnS NPs were prepared as follows: 50 mL of 0.5 M zinc acetate solution was prepared with deionized water and stirred in a glass beaker to dissolve zinc acetate. In a separate beaker, 50 mL of 0.5 M of sodium sulphide was prepared and poured into 100 mL of deionized water with 3.0 g PVP and stirred until all solids were dissolved. The zinc acetate solution was then added to the sodium sulphide solution dropwise while stirring at room temperature. The resulting precipitate was then filtered under reduced pressure and washed with distilled water and twice with ethanol to remove sodium ions. Finally, the resulting ZnS nanoparticles were then dried in oven at 100 °C for 3 h. The morphology and elemental composition of the ZnS NPs powder were investigated using a scanning electron microscopy (SEM) and energy-dispersive X-ray spectroscopy (EDAX) analysis. X-ray diffraction data of ZnS were then acquired on a PANalytical Empyrean diffractometer operated at 45 kV and 40 mA. The pattern was collected from 2θ values of 20 to 60°, step size of 0.02° and an acquisition time of 127 s per step.

2.3 Device fabrication

P3HT:PCBM-based organic solar cells mixed with ZnS plasmonic nanoparticles were fabricated on unpatterned ITO-coated glass substrates. The substrates were first partially etched with acid solution (HCL:H_2O:HNO_3 at 48%:48%:4%) to remove part of the ITO. They were then successively cleaned in ultrasonic bath with detergent, distilled water, acetone and isopropanol, respectively, for 10 min waiting time. The samples were then dried in an oven at 120 °C for 30 min. A thin layer of PEDOT:PSS was spin coated onto the samples at 3500 rpm. The samples were dried again in the oven under ambient atmosphere. Three P3HT:PCBM (1:1) blend solutions with 3 wt%, 5 wt% or 8 wt% of ZnS NPs were prepared in chloroform and sonicated for 3 h at 40 °C to ensure good dispersion of the NPs and miscibility of the polymer-fullerene blend. The P3HT:PCBM solutions incorporated with ZnS NPs were then spin coated onto the PEDOT:PSS film at 1300 rpm for 40 s. The samples were then dried in an oven under nitrogen atmosphere for 10 min before being transferred into a vacuum deposition chamber (Edwards Auto 306) for deposition of lithium fluoride (LiF) and aluminium (Al). Thin layers of LiF (0.5 nm) and Al (80 nm) were deposited onto the samples at a base pressure of 10^{-6} mbar resulting in devices with the following structure: ITO/PEDOT:PSS/P3HT:PCBM:NP/LiF/Al. Schematic diagram for device structure depicted in Fig. 3a shows the various layers of the organic solar cell based on ZnS plasmonic nanoparticles incorporated into P3HT:PCBM active layer.

3 Results and discussion

3.1 XRD analysis of ZnS NPs

The newly synthesized zinc sulphide powder was characterized in terms of its morphological and optical properties. The XRD pattern presented in Fig. 1 was taken from ZnS NPs powder which clearly showed well known diffraction peaks of the compound. The measured diffraction pattern matched very well with ICDD data card no.: 01-074-4985. Three prominent diffraction peaks are observed at 2θ values of 28.85°, 47.81° and 56.54°. These diffraction peaks correspond to the reflections of the beam from the (111), (220) and (311) planes of the cubic phase of ZnS. The interplanar spacings (d_{hkl}) corresponding to these XRD peaks are given in Table 1. The d-spacing obtained of the three prominent peaks matches

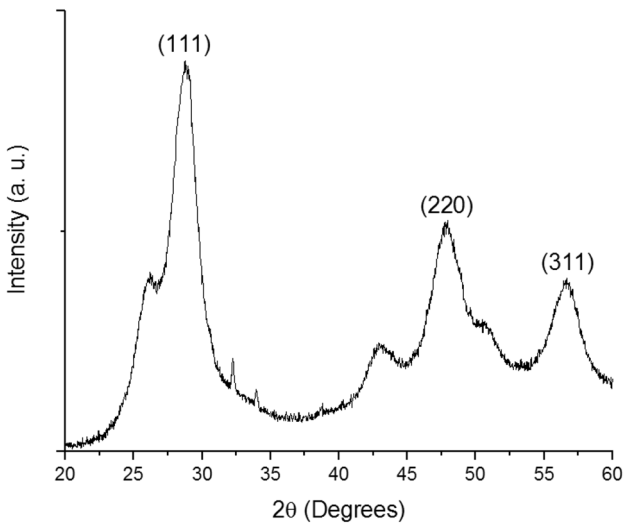

Fig. 1 X-ray diffraction pattern for ZnS nanoparticles

very well with the literature results of 3.07 Å, 1.89 Å and 1.59 Å from Saravanan et al. which matched very well with JCPDS data card no.: 79-0043 [14]. Kannappan et al. also observed similar diffraction peaks of solid state synthesized ZnS NPs at 2θ values of 28.51°, 47.91° and 56.56° [17]. The d-spacing of 3.07 Å obtained by calculation using the X-ray measurement data matches closely with the value of 3.10 Å obtained by TEM measurements (see red circle in Fig. 2b). The crystalline sizes (D_{size}) of the ZnS NPs were calculated using the Debye–Scherrer equation:

$$D_{size} = \frac{0.91\lambda}{\beta(2\theta)cos(\theta)} \quad (1)$$

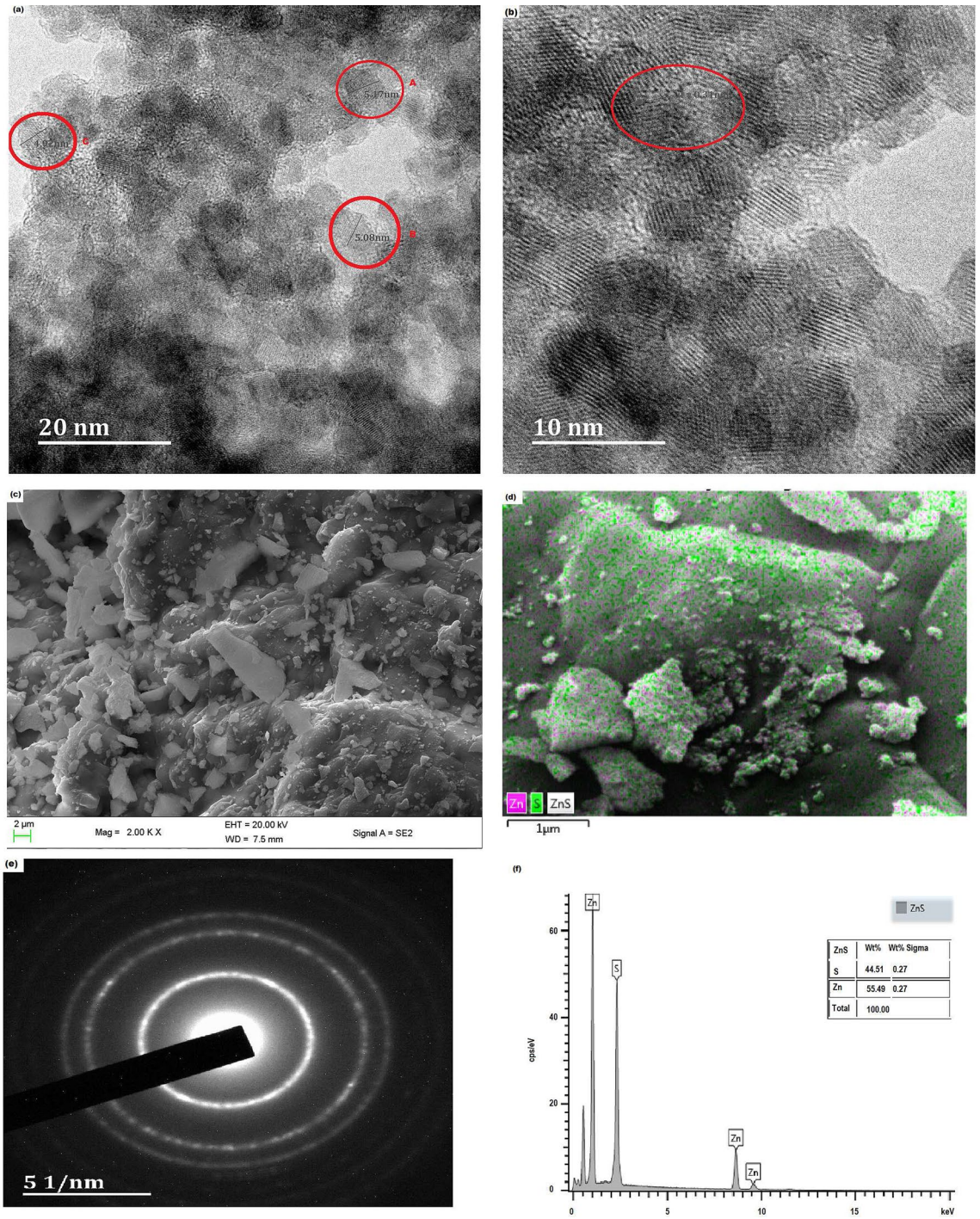

Fig. 2 **a**, **b** HRTEM images, **c**, **d** HRSEM, **e** SAED pattern images of ZnS nanoparticles and **f** the EDX of the ZnS NPs

where λ (0.15406 nm) is the wavelength of the X-rays, β is the full width at half maximum in radians. The reflections from the (111), (220) and (311) planes, occurring at 2θ at 28.85° , 47.81° and 56.54°, respectively, were used for the crystalline size calculation and the results are shown in Table 1.

The D_{size} of 5.10 nm at $2\theta = 28.85°$ matches very well with particle size determined using TEM (see circles A and B in Fig. 2a). The crystalline domain sizes obtained are not consistent suggesting that the sample contains non-uniform particles. This is also supported by the TEM measurements with crystallite sizes close to 5.0 nm.

It has been reported that nano-sized ZnS mostly synthesized by colloid chemistry usually have the cubic zincblende structure which is a stable phase at low temperatures for ZnS [16]. We used the standard formula for a cubic structure to determine the average lattice constant a to be $a = 5.366$ Å. This value falls within the range of ZnS NPs lattice constants a= 5.317 Å [14]($a = 5.318$ ÅJCPDS card no.: 79-0043) and $a = 5.40$ Å [18] reported in the literature.

$$\frac{1}{d_{hkl}^2} = \frac{h^2 + k^2 + l^2}{a^2} \tag{2}$$

3.2 SEM and TEM electron microscopy

The microstructure and morphology of the synthesized zinc sulphide (ZnS) nanoparticles (NPs) were investigated by scanning electron microscopy (SEM) and high-resolution transmission electron microscopy (HRTEM). The HRTEM image provided in Fig. 2(a,b) show a two-dimensional disc-like structures with well-aligned crystal fringes as presented in (b). The crystallite size range of 5–8 nm which is consistent with the observation in XRD measurements. The SEM image provided in Fig. 2c indicated the formation of large clusters of the metal composite in extended space. The elemental mapping of the composite was also taken using EDX analysis suggesting a uniform distribution of the elements zinc and sulphur in the region (see Fig. 2d). Furthermore, the EDX data provided in Fig. 2f indicated that the element zinc and sulphur existed in the synthesized powder with the proportion of 55.49% zinc, 44.51% sulphur. This confirms the absence of any impurity in the nanoparticles.

3.3 Electrical properties

The current–voltage (J–V) characteristics of the devices were measured using a computer-interfaced Keithley 2420 sourcemeter under standard light illumination using a solar simulator at AM1.5 operating at an integrated power intensity of 100 mW cm^{-2} (see Fig. 3). The solar absorber layers of the devices were subject to high doping level of ZnS at the concentration from 0 % to 8% in P3HT:PCBM blend. The J–V characteristics of the solar cells showed a remarkable increase on the short-circuit current and fill-factor (FF) compared to undoped solar absorber layer (see Table 2). This high FF is as a result of improved charge carrier mobilities and reduced recombination in the OPV devices. It has been reported that if charge generation changes significantly between open-circuit conditions and short-circuit conditions, then this would influence the device FF and such field-dependent charge carrier generation has been shown to be the main determinant in some donor/acceptor combinations [19–21]. Lakhwani et al. reported that for most high efficiency OPV systems, geminate recombination is greatly reduced and bimolecular recombination is the main mechanism for charge recombination [22]. Therefore, it is the ratio of recombination and extraction of charge carriers that principally determines the dependence of the photocurrent on bias, and hence the FF [23].

Table 1 Interplanar spacing (d_{hkl}) from XRD data card with corresponding (hkl) and lattice parameter values for ZnS

Pos. (2θ)	FWHM	hkl	d_{hkl} (Å)	a (Å)	D_{size} (nm)
28.85	1.6265	111	3.09	5.35	5.10
47.81	2.8259	220	1.90	5.37	3.11
56.54	2.6397	311	1.63	5.37	3.46

The devices with 8 wt% ZnS NPs in its active layer showed very high photocurrent collection and witnessed reduction in the device fill-factor. This could be attributed to the loss of shunt resistance due to the presence of high concentrations of ZnS. The V_{oc} of all devices exhibited minor changes ranging between 0.55 and 0.59 V. The highest open-circuit voltage and fill-factor were recorded from the solar cells that contains 5s% concentration of ZnS. This suggest that the optimum amount of 8 wt% ZnS nanoparticles not only assisted charge generation but also improved the interfacial conditions between the active layer and the electrodes which is responsible for high V_{oc}.

In other words, the ZnS NPs did not introduce significant defect density (energy disorder) that negatively affected the HOMO and LUMO levels of the polymer blend. However, 5 wt% was not sufficient to warrant high short-circuit current and best efficiency as recorded in Table 2. The highest current density measured from the solar cells was at the 8% concentration of ZnS in the photoactive medium which is as high as 15.65 mA cm^{-2} and PCE is 4%. The electrical properties of the devices are shown in Fig. 3b–d. It is noted here that the dopant concentrations greater than 8 wt% were detrimental to the device performances. However, the enhanced device performance is attributed to the occurrence of near-field enhancement at the vicinity of the small diameter ZnS NPs as well as forward scattering from the larger

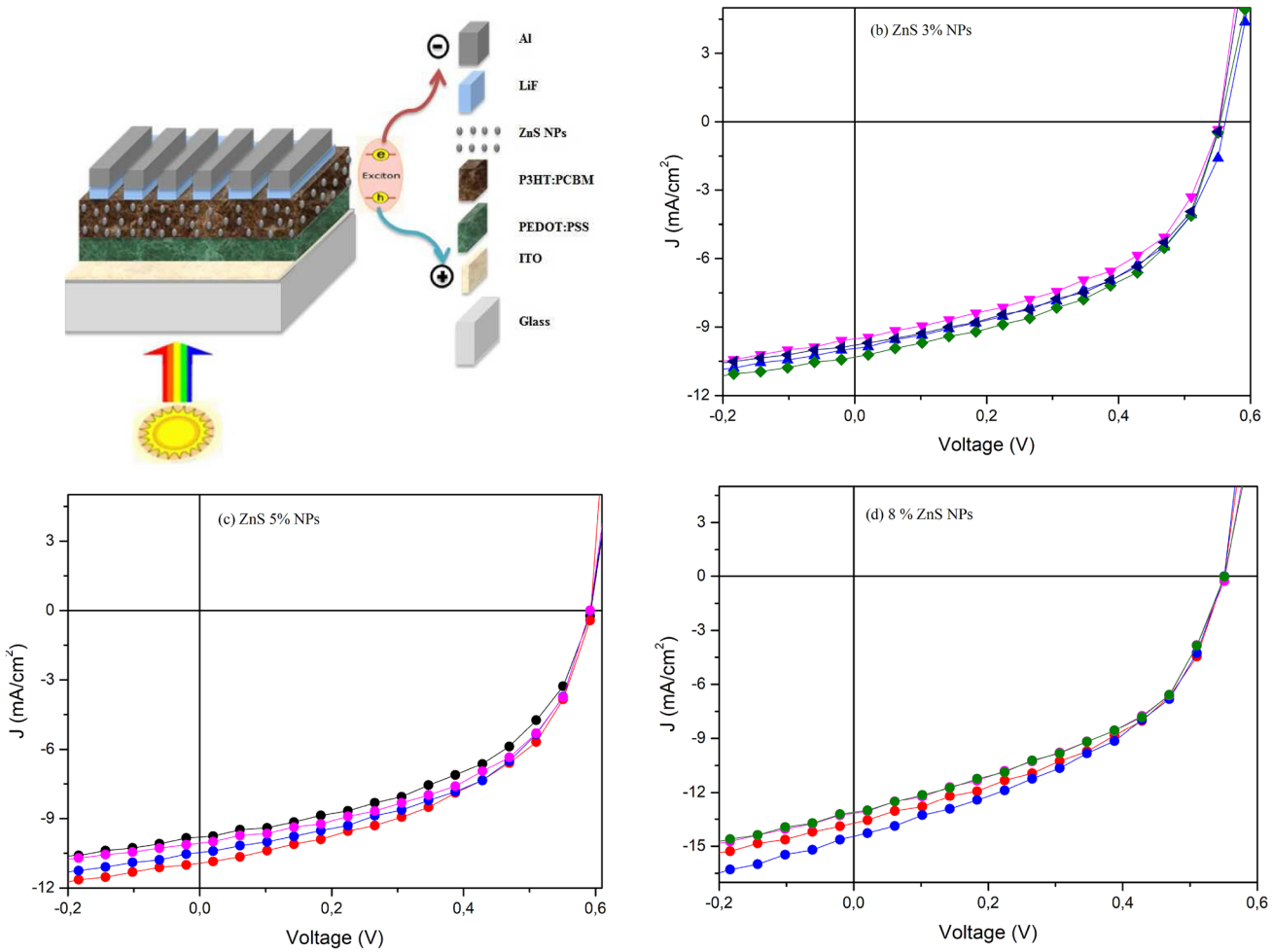

Fig. 3 Schematic diagram **a** of the OPV devices, **b–d** current–voltage characteristics of P3HT:PCBM-based organic solar cells

Table 2 Summary of the best device performance of the solar cells based on P3HT:PCBM blend at different concentrations of ZnS

Device (%)	V_{oc} (V)	J_{sc} (mA cm^{-2})	FF (%)	PCE (%)	μ_o (cm^{-2} V$^{-\frac{1}{2}}$ s^{-1})
Pristine	0.56	7.50	45.00	1.90	1.83×10^{-5}
3%	0.55	10.41	50.87	2.93	2.09×10^{-2}
5%	0.59	10.89	48.91	3.16	6.00×10^{-2}
8%	0.55	15.65	46.43	4.00	1.46×10^{-2}

diameter ZnS NPs, which improves optical path length and optical absorption in the photoactive layer. The performance data shown in Table 2 show a strong correlation between the solar cell performance and the ZnS NPs concentration in the photoactive layer blend, where the NPs concentration is varied from 0 wt%(pristine devices) to 8 wt% that enhanced the overall device performance. It has been reported that charge carrier mobility imbalance in P3HT:PCBM OPVs negatively affects their performance [9]. The short-circuit current density (J_{sc}) and FF enhancements observed suggest that the incorporation of the plasmonic NPs helped improve the charge carrier mobility imbalance between the electron and hole mobilities. As a result of the enhancements on the J_{sc} and FF, the PCE of the OPV devices improved from 1.9% to as high as 4.0%. This is a remarkable enhancement considering the fact that the devices were fabricated under ambient conditions with no use of a glove box filled with inert gases.

3.4 Optical absorption of the photoactive film

The UV–Vis spectra of the photoactive films composed of P3HT:PCBM blend were taken with and without the inclusion of ZnS (see Fig 4a). The absorption spectrum of the

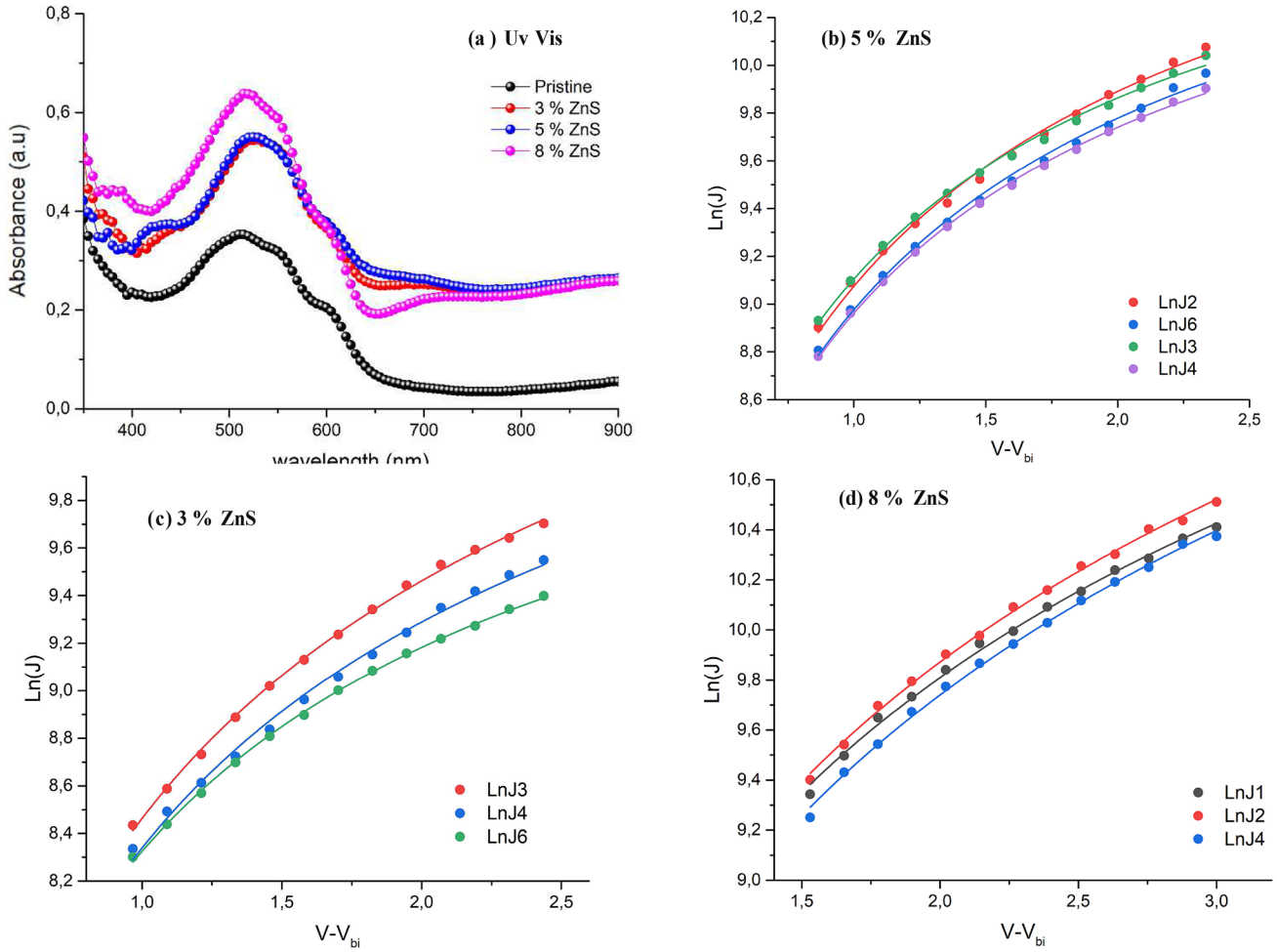

Fig. 4 **a** Optical absorption spectra of the P3HT:PCBM blend films. **b–d** are the charge transport properties obtained from space charge limited current data which are compared with Mott–Gurney Law

pristine film shows the typical P3HT:PCBM blend absorption spectrum with broad absorption peak centred around 510 nm and two vibronic shoulders at 555 nm and 605 nm. The absorption spectra of the blend films containing ZnS NPs at different concentrations show two bums located at 400 nm and above 700 nm. The peaks of the absorption spectra are generally red-shifted with respect to those of pristine film. The maximum absorption peaks are centred between 520 and 530 nm. The two vibronic shoulders are still distinctly visible even with those films containing ZnS. This suggests that the crystallinity of the P3HT:PCBM films was not disturbed by the incorporation of the ZnS NPs. The effect of red shift of the absorption spectra observed in the NPs-doped blend films is attributed to the interaction of ZnS with sulphur-rich back bone of the polymer chain. The red shift is in fact favourable since it repositions the absorption peak to an intense emission spectrum of the solar radiation. Furthermore, the ZnS NPs-doped films absorption observed, above 700 nm wavelength, is likely to come from the photons scattered at near-infrared regions. This is evident from the absorbance at the highest concentration of ZnS in the medium (8%). Plasmonic NPs in the photoactive layer of OPVs can remarkably enhance optical absorption, either via the formation of scattered waves by the larger diameter NPs or/and due to the LSPR modes excitation at the smaller diameter NPs [9, 24, 25]. Therefore, the enhanced optical absorption observed in the blend films containing the nanoparticles can be attributed to the forward light scattering and LSPR effect from the ZnS NPs.

3.5 Charge transport

The current–voltage characteristics of the OPV devices under dark illumination were used to study the charge transport properties of the devices. The measured space charge limited current (SCLC) was fitted to the Mott–Gurney law (Eq. 2) to determine the charge transport properties. The

SCLC is often described by the Mott–Gurney law using the field-dependent mobility equation [9]:

$$J = \frac{9}{8}\varepsilon\varepsilon_o\mu_o \exp\left(0.89\gamma\sqrt{\frac{V}{L}}\right)\frac{V^2}{L^3} \quad (3)$$

where ε is the relative dielectric permittivity of the material, ε_o is the permittivity of free space, L is the active layer thickness, γ is the field activation factor and V is the voltage drop across the sample corrected by the built-in voltage (V_{bi}). The experimental data were fitted with the natural logarithm of Eq. 2 to obtain charge mobilities of the device samples and the resultant mobilities are shown in Table 2. The experimental data agreed very well with the model as shown in Fig. 4b–d. The charge mobility values showed three orders of magnitude increase when plasmonic ZnS NPs were incorporated in the active layer of the devices. This observation suggests that germinate recombination in the devices was significantly reduced. It has been reported that a strong imbalance between the electron and hole charge carriers leads to space charge photocurrents, characterized by a square root dependence on applied voltage [26], which then limits the FF to about 40% [27, 28]. It was observed in our experimental results for 3 wt% and 5 wt% ZnS NPs concentration that the enhanced charge carrier mobilities were accompanied by significant enhancements of the device FFs. However, the increase in charge carrier mobility in the devices with 8 wt% ZnS NPs concentration did not bring about significant increase in the device FFs compared to the pristine devices. Thermal annealing applied on the devices may have also contributed in the enhancement of the charge carrier mobility due to the self-organisation into crystalline structure of the regioregular polymer (P3HT).

4 Conclusion

Nanostructured ZnS NPs with average lattice parameter of $a = 5.3663$ Å were successfully synthesized by colloidal chemistry. The nanoparticles were used in the solar absorber layer of thin film organic solar cell at various concentrations from (0–8) wt%. The evidence found from the experiment suggest that all devices fabricated with ZnS has shown improved performance compared to the undoped ones. Moreover, the incorporation of the NPs did not negatively affect the crystallinity of the polymers blend as evidenced from optical absorption of doped P3HT:PCBM films. The newly fabricated polymer solar cell exhibited remarkable enhancement in the measured photocurrent, fill-factor and open-circuit voltage. The best device performance was obtained at 8 wt% ZnS NPs concentration which resulted in a maximum J_{sc} of 15.65 mA cm^{-2} and highest PCE of 4.0%. The occurrence of the near-field at the site of metal NPs facilitated fast exciton dissociation in the medium as well as enhanced photocurrent collection. It is to be noted here that the light scattering effect from metallic NPs increased path length thereby more photons are absorbed.

Acknowledgements This work is financially supported by National Research Foundation (NRF), South Africa. The authors also grateful to members of staff of Materials Characterisation section at National Metrology Institute of South Africa (NMISA), Microscopy and Microanalysis Unit (MMU) at the School of Life Sciences in the University of KwaZulu-Natal for SEM, XRD and EDX analysis.

Funding Funding was provided by National Research Foundation South Africa (Grant No. 113831).

References

1. W. Ma, C. Yang, X. Gong, K. Lee, A.J. Heeger, Thermally stable, efficient polymer solar cells with nanoscale control of the interpenetrating network morphology. Adv. Funct. Mater. **15**(10), 1617–1622 (2005)
2. A. Hayakawa, O. Yoshikawa, T. Fujieda, K. Uehara, S. Yoshikawa, High performance polythiophene/fullerene bulk-heterojunction solar cell with a TiO_x hole blocking layer. Appl. Phys. Lett. **90**(16), 163517 (2007)
3. G. Li, V. Shrotriya, J. Huang, Y. Yao, T. Moriarty, K. Emery, Y. Yang, High-efficiency solution processable polymer photovoltaic cells by self-organization of polymer blends, in *Materials For Sustainable Energy: A Collection of Peer-Reviewed Research and Review Articles*, ed. by V. Dusastre (Nature Publishing Group, Berlin, 2011), pp. 80–84
4. M.S.G. Hamed, S.O. Oseni, A. Kumar, Nickel sulphide nanocomposite assisted hole transport in thin film polymer solar cells. Sol. Energy **195**, 310–317 (2020)
5. S.K. Jang, S.C. Gong, H.J. Chang, Effects of various solvent addition on crystal and electrical properties of organic solar cells with P3HT: PCBM active layer. Synth. Met. **162**(5–6), 426–430 (2012)
6. G. Zhao, Y. He, Y. Li, 6.5% efficiency of polymer solar cells based on poly (3-hexylthiophene) and indene–C_{60} bisadduct by device optimization. Adv. Mater. **22**(39), 4355–4358 (2010)
7. T.A. Kareem, A.A. Kaliani, Fabrication and characterization of ZnSCubic: P3HT, ZnSHexa: P3HT and ZnSHexa: P3HT: PVA-Ag bulk heterojunction solar cells. J. Nano Electr. Phys. **7**(2), 1–6 (2015)
8. L. Lu, Z. Luo, T. Xu, L. Yu, Cooperative plasmonic effect of Ag and Au nanoparticles on enhancing performance of polymer solar cells. Nano Lett. **13**(1), 59–64 (2012)
9. M.W. Dlamini, G.T. Mola, Near-field enhanced performance of organic photovoltaic cells. Physica B **552**, 78–83 (2019)
10. E.A.A. Arbab, G.T. Mola, Metals decorated nanocomposite assisted charge transport in polymer solar cell. Mater. Sci. Semicond. Process. **91**, 1–8 (2019)
11. D.D. Fung, L. Qiao, W.C. Choy, C. Wang, E.I. Wei, F. Xie, S. He, Optical and electrical properties of efficiency enhanced polymer solar cells with Au nanoparticles in a PEDOT-PSS layer. J. Mater. Chem. **21**(41), 16349–16356 (2011)
12. Y.Y. She, Y.A.N.G. Juan, K.Q. Qiu, Synthesis of ZnS nanoparticles by solid–liquid chemical reaction with ZnO and Na2S under ultrasonic. Trans. Nonferr. Metals Soc. China **20**, s211–s215 (2010)
13. M. Bredol, K. Matras, A. Szatkowski, J. Sanetra, A. Prodi-Schwab, P3HT/ZnS: a new hybrid bulk heterojunction photovoltaic system

with very high open circuit voltage. Sol. Energy Mater. Sol. Cells **93**(5), 662–666 (2009)
14. N. Saravanan, G.B. Teh, S.Y.P. Yap, K.M. Cheong, Simple synthesis of ZnS nanoparticles in alkaline medium. J. Mater. Sci. **19**(12), 1206–1208 (2008)
15. P. D'Amico, A. Calzolari, A. Ruini, A. Catellani, New energy with ZnS: novel applications for a standard transparent compound. Sci. Rep. **7**(1), 16805 (2017)
16. Y. Zhao, Y. Zhang, H. Zhu, G.C. Hadjipanayis, J.Q. Xiao, Low-temperature synthesis of hexagonal (wurtzite) ZnS nanocrystals. J. Am. Chem. Soc. **126**(22), 6874–6875 (2004)
17. P. Kannappan, R. Dhanasekaran, Structural and optical characterization of ZnS nanoparticles synthesized by low temperature. Int. J. Recent Technol. Eng. **7**(4S), 26–28 (2018)
18. C.S. Pathak, M.K. Mandal, V. Agarwala, Synthesis and characterization of zinc sulphide nanoparticles prepared by mechanochemical route. Superlatt. Microstruct. **58**, 135–143 (2013)
19. D. Bartesaghi, I. del Carmen Pérez, J. Kniepert, S. Roland, M. Turbiez, D. Neher, L.J.A. Koster, Competition between recombination and extraction of free charges determines the fill factor of organic solar cells. Nat. Commun. **6**, 7083 (2015)
20. G.F. Dibb, F.C. Jamieson, A. Maurano, J. Nelson, J.R. Durrant, Limits on the fill factor in organic photovoltaics: distinguishing nongeminate and geminate recombination mechanisms. J. Phys. Chem. Lett. **4**(5), 803–808 (2013)
21. S. Albrecht, S. Janietz, W. Schindler, J. Frisch, J. Kurpiers, J. Kniepert, S. Inal, P. Pingel, K. Fostiropoulos, N. Koch, D. Neher, Fluorinated copolymer PCPDTBT with enhanced open-circuit voltage and reduced recombination for highly efficient polymer solar cells. J. Am. Chem. Soc. **134**(36), 14932–14944 (2012)
22. G. Lakhwani, A. Rao, R.H. Friend, Bimolecular recombination in organic photovoltaics. Annu. Rev. Phys. Chem. **65**, 557–581 (2014)
23. R. Mauer, I.A. Howard, F. Laquai, Effect of nongeminate recombination on fill factor in polythiophene/methanofullerene organic solar cells. J. Phys. Chem. Lett **1**(24), 3500–3505 (2010)
24. M.D. Brown, T. Suteewong, R.S.S. Kumar, V. D'Innocenzo, A. Petrozza, M.M. Lee, U. Wiesner, H.J. Snaith, Plasmonic dye-sensitized solar cells using core–shell metal–insulator nanoparticles. Nano Lett. **11**(2), 438–445 (2010)
25. K. Ueno, T. Oshikiri, Q. Sun, X. Shi, H. Misawa, Solid-state plasmonic solar cells. Chem. Rev. **118**(6), 2955–2993 (2017). https://doi.org/10.1021/acs.chemrev.7b00235
26. V.D. Mihailetchi, J. Wildeman, P.W.M. Blom, Space-charge limited photocurrent. Phys. Rev. Lett. **94**(12), 126602 (2005)
27. M. Lenes, M. Morana, C.J. Brabec, P.W. Blom, Recombination-limited photocurrents in low bandgap polymer/fullerene solar cells. Adv. Funct. Mater. **19**(7), 1106–1111 (2009)
28. S.O. Oseni, G.T. Mola, The effect of uni- and binary solvent additives in PTB7:PC61BM based solar cells. Sol. Energy **150**, 66–72 (2017)